

Nonlinear Dynamics of A Damped Magnetic Oscillator

Sang-Yoon Kim *

Department of Physics

Kangwon National University

Chunchon, Kangwon-Do 200-701, Korea

We consider a damped magnetic oscillator, consisting of a permanent magnet in a periodically oscillating magnetic field. A detailed investigation of the dynamics of this dissipative magnetic system is made by varying the field amplitude A . As A is increased, the damped magnetic oscillator, albeit simple looking, exhibits rich dynamical behaviors such as symmetry-breaking pitchfork bifurcations, period-doubling transitions to chaos, symmetry-restoring attractor-merging crises, and saddle-node bifurcations giving rise to new periodic attractors. Besides these familiar behaviors, a cascade of “resurrections” (i.e., an infinite sequence of alternating restabilizations and destabilizations) of the stationary points also occurs. It is found that the stationary points restabilize (destabilize) through alternating subcritical (supercritical) period-doubling and pitchfork bifurcations. We also discuss the critical behaviors in the period-doubling cascades.

PACS numbers: 05.45.-a, 05.45.Ac

I. INTRODUCTION

We consider a permanent magnet of dipole moment m placed in a periodically oscillating magnetic field. This magnetic oscillator (MO) can be described by a second-order non-autonomous ordinary differential equation [1–3],

$$I\ddot{\theta} + b\dot{\theta} + mB_0 \cos \omega t \sin \theta = 0, \quad (1)$$

where the overdot denotes the differentiation with respect to time, θ is the angle between the permanent magnet and the magnetic field, I is the moment of inertia about a rotation axis, b is the damping parameter, and B_0 and ω are the amplitude and frequency of the periodically oscillating magnetic field, respectively.

Making the normalization $\omega t \rightarrow 2\pi(t + \frac{1}{2})$ and $\theta \rightarrow 2\pi x$, we obtain a dimensionless form of Eq. (1),

$$\ddot{x} + \Gamma \dot{x} - A \cos 2\pi t \sin 2\pi x = 0, \quad (2)$$

where x is a normalized angle with mod 1, $\Gamma = 2\pi b/I\omega$ and $A = 2\pi mB_0/I\omega^2$. Note also that Eq. (2) describes the motion of a particle in a standing wave field [4–6]. For the conservative case of $\Gamma = 0$, the Hamiltonian system exhibits period-doubling bifurcations and large-scale stochasticity as the normalized field amplitude A is increased, which have been found both experimentally [1–3] and theoretically [4–6]. Here we are interested in the damped case of $\Gamma \neq 0$ and make a detailed investigation of the dynamical behaviors of the damped MO by varying the amplitude A .

This paper is organized as follows. We first discuss bifurcations associated with stability of periodic orbits

and Lyapunov exponents in the damped MO in Sec. II. With increasing A up to sufficiently large values, dynamical behaviors of the damped MO are then investigated in Sec. III. This very simple-looking damped MO shows a richness in its dynamical behaviors. As A is increased, breakdown of symmetries via pitchfork bifurcations [8], period-doubling transitions to chaos [9], restoration of symmetries via attractor-merging crises [10], birth of new periodic attractors through saddle-node bifurcations [8], and so on are numerically found. In addition to these familiar behaviors, the stationary points exhibit a cascade of “resurrections” [11] (i.e., they restabilize after their instability, destabilize again, and so forth *ad infinitum*). It is found that the restabilizations (destabilizations) occur via alternating subcritical (supercritical) period-doubling and pitchfork bifurcations. An infinite sequence of period-doubling bifurcations, leading to chaos, also follows each destabilization of the stationary points. In Sec. IV, we also study the critical scaling behaviors in the period-doubling cascades. It is found that the critical behaviors are the same as those for the one-dimensional (1D) maps [9]. Finally, a summary is given in Sec. V.

II. STABILITY, BIFURCATIONS AND LYAPUNOV EXPONENTS

In this section we first discuss stability of periodic orbits in the damped MO, using the Floquet theory [12]. Bifurcations associated with the stability and Lyapunov exponents are then discussed.

The second-order ordinary differential equation (2)

*Electronic address: sykim@cc.kangwon.ac.kr

is reduced to two first-order ordinary differential equations:

$$\dot{x} = y, \quad (3a)$$

$$\dot{y} = -\Gamma y + A \cos 2\pi t \sin 2\pi x. \quad (3b)$$

These equations have two symmetries S_1 and S_2 , because the transformations

$$S_1 : x \rightarrow x \pm \frac{1}{2}, y \rightarrow y, t \rightarrow t \pm \frac{1}{2}, \quad (4)$$

$$S_2 : x \rightarrow -x, y \rightarrow -y, t \rightarrow t, \quad (5)$$

leave Eq. (3) invariant. The transformations in Eqs. (4) and (5) are just the shift in both x and t and the (space) inversion, respectively. Hereafter, we will call S_1 and S_2 the shift and inversion symmetries, respectively. If an orbit $z(t) [= (x(y), y(t))]$ is invariant under S_i ($i = 1, 2$), it is called an S_i -symmetric orbit. Otherwise, it is called an S_i -asymmetric orbit and has its ‘‘conjugate’’ orbit $S_i z(t)$.

The phase space of the damped MO is three dimensional with the coordinates x , y , and t . Since the damped MO is periodic in t , it is convenient to regard time as a circular coordinate (with mod 1) in the phase space. We then consider the surface of section, the $x - y$ plane at interger times (i.e., $t = m$, m : integer). The phase-space trajectory intersects this plane in a sequence of points. This sequence of points corresponds to a mapping on the plane. This map plot of an initial point $z_0 [= (x_0, y_0)]$ can be conveniently generated by sampling the orbit points z_m at the discrete time $t = m$. We call the transformation $z_m \rightarrow z_{m+1}$ the Poincaré map and write $z_{m+1} = P(z_m)$.

The linear stability of a q -periodic orbit of P such that $P^q(z_0) = z_0$ is determined from the linearized-map matrix $DP^q(z_0)$ of P^q at an orbit point z_0 . Here P^q means the q -times iterated map. Using the Floquet theory, the matrix M ($\equiv DP^q$) can be obtained by integrating the linearized equations for small displacements,

$$\delta\dot{x} = \delta y, \quad (6a)$$

$$\delta\dot{y} = -\Gamma\delta y + 2\pi A \cos 2\pi t \cos 2\pi x \delta x \quad (6b)$$

with two initial displacements $(\delta x, \delta y) = (1, 0)$ and $(0, 1)$ over the period q . The eigenvalues, λ_1 and λ_2 , of M are called the Floquet (stability) multipliers, characterizing the orbit stability. By using the Liouville’s formula [7], we obtain the determinant of M ($\det M$),

$$\det M = e^{-\Gamma q}. \quad (7)$$

Hence the pair of Floquet multipliers of a periodic orbit lies either on the circle of radius $e^{-\Gamma q/2}$ or on the real axis in the complex plane. The periodic orbit is stable when both multipliers lie inside the unit circle. We first note that they never cross the unit circle, except at the real axis and hence Hopf bifurcations do not occur. Consequently, it can lose its stability only when a Floquet multiplier decreases (increases) through -1 (1) on the real axis. When a Floquet multiplier λ decreases through -1 ,

the periodic orbit loses its stability via period-doubling bifurcation. On the other hand, when a Floquet multiplier λ increases through 1 , it becomes unstable via pitchfork or saddle-node bifurcation. For each case of the period-doubling and pitchfork bifurcations, two types of supercritical and subcritical bifurcations occur. For more details on bifurcations, refer to Ref. [8].

Lyapunov exponents of an orbit $\{z_m\}$ in the Poincaré map P characterize the mean exponential rate of divergence of nearby orbits [13]. There exist two Lyapunov exponents σ_1 and σ_2 ($\sigma_1 \geq \sigma_2$) such that $\sigma_1 + \sigma_2 = -\Gamma$, because the linearized Poincaré map DP has a constant Jacobian determinant, $\det DP = e^{-\Gamma}$. We choose an initial perturbation δz_0 to the initial orbit point z_0 and iterate the linearized map DP for δz along the orbit to obtain the magnitude d_m ($\equiv |\delta z_m|$) of δz_m . Then, for almost all infinitesimally-small initial perturbations, we have the largest Lyapunov exponent σ_1 given by

$$\sigma_1 = \lim_{m \rightarrow \infty} \frac{1}{m} \ln \frac{d_m}{d_0}. \quad (8)$$

If σ_1 is positive, then the orbit is called a chaotic orbit; otherwise, it is called a regular orbit.

III. RICH DYNAMICAL BEHAVIORS OF THE DAMPED MO

In this section, by varying the amplitude A , we investigate the evolutions of both the stationary points and the rotational orbits of period 1 in the damped MO for a moderately damped case of $\Gamma = 1.38$. As A is increased, the damped MO, albeit simple looking, exhibits rich dynamical behaviors, such as symmetry-breaking pitchfork bifurcations, period-doubling transitions to chaos, symmetry-restoring attractor-merging crises, and saddle-node bifurcations giving rise to new periodic attractors. In addition to these familiar behaviors, the stationary points also undergo a cascade of resurrections (i.e. an infinite sequence of alternating restabilizations and destabilizations). It is found that the restabilizations (destabilizations) occur via alternating subcritical (supercritical) period-doubling and pitchfork bifurcations. An infinite sequence of period-doubling bifurcations, leading to chaos, also follows each destabilization of the stationary points.

A. Evolution of the stationary points

We first consider the case of the stationary points. The damped MO has two stationary points \hat{z} ’s. One is $\hat{z}_I = (0, 0)$, and the other one is $\hat{z}_{II} = (\frac{1}{2}, 0)$. These stationary points are symmetric ones with respect to the inversion symmetry S_2 , while they are asymmetric and conjugate ones with respect to the shift symmetry S_1 . Hence they are partially symmetric orbits with only the

inversion symmetry S_2 . We also note that the two stationary points are the fixed points of the Poincaré map P [i.e., $P(\hat{z}) = \hat{z}$ ($\hat{z} = \hat{z}_I, \hat{z}_{II}$)].

With increasing A we investigate the evolution of the two fixed points \hat{z}_I and \hat{z}_{II} . Two bifurcation diagrams starting from \hat{z}_I and \hat{z}_{II} are given in Figs. 1(a) and 1(b), respectively. Each fixed point loses its stability via symmetry-conserving period-doubling bifurcation, giving rise to a stable S_2 -symmetric orbit with period 2. However, as A is further increased each S_2 -symmetric orbit of period 2 becomes unstable by a symmetry-breaking pitchfork bifurcation, leading to the birth of a conjugate pair of S_2 -asymmetric orbits of period 2. (For the sake of convenience, only one S_2 -asymmetric orbit of period 2 is shown.) After breakdown of the S_2 symmetry, each 2-periodic orbit with completely broken symmetries exhibits an infinite sequence of period-doubling bifurcations, ending at a finite critical point $A_{s,1}^*$ ($= 3.934787 \dots$). The critical scaling behaviors near the critical point $A_{s,1}^*$ are the same as those for the 1D maps [9], as will be seen in Sec. IV.

After the period-doubling transition to chaos, four small chaotic attractors with completely broken symmetries appear; they are related with respect to the two symmetries S_1 and S_2 . As A is increased the different parts of each chaotic attractor coalesce and form larger pieces. For example, two chaotic attractors with σ_1 (largest Lyapunov exponent) $\simeq 0.11$, denoted by c_1 and c_2 , near the unstable stationary point \hat{z}_I are shown in Fig. 2(a) for $A = 3.937$; their conjugate chaotic attractors with respect to the S_1 symmetry near the unstable stationary point \hat{z}_{II} are not shown. Each one is composed of four distinct pieces. However, as A is further increased these pieces also merge into two larger pieces. An example with $\sigma_1 \simeq 0.18$ is shown in Fig. 2(b) for $A = 3.94$.

As A exceeds a critical value ($\simeq 3.9484$), the two chaotic attractors c_1 and c_2 in Fig. 2(b) merge into a larger one c through an S_2 -symmetry-restoring attractor-merging crisis. For example, a chaotic attractor c with $\sigma_1 \simeq 0.37$ and its conjugate one, denoted by s , with respect to the S_1 symmetry are shown in Fig. 3(a) for $A = 3.96$. These two chaotic attractors c and s are S_2 -symmetric ones, although they are still S_1 -asymmetric and conjugate ones. Thus the inversion symmetry S_2 is first restored. However, as A increases through a second critical value ($\simeq 3.9672$), the two small chaotic attractors c and s also merge into a larger one via S_1 -symmetry-restoring attractor-merging crisis, as shown in Fig. 3(b) for $A = 3.98$. Note that the single large chaotic attractor with $\sigma \simeq 0.64$ is both S_1 - and S_2 -symmetric one. Consequently, the two symmetries S_1 and S_2 are completely restored, one by one through two successive symmetry-restoring attractor-merging crises. However, this large chaotic attractor disappears for $A \simeq 4.513$, and then the system is asymptotically attracted to a stable rotational orbit of period 1 born through a saddle-node bifurcation, as shown in Fig. 4.

B. Evolution of the rotational orbits

We now investigate the evolution of the rotational orbits of period 1. A pair of stable and unstable rotational orbits with period 1 is born for $A \simeq 2.771$ via saddle-node bifurcation. In contrast to the stationary points, these rotational orbits are S_1 -symmetric, but S_2 -asymmetric and conjugate, ones. The bifurcation diagram starting from a stable rotational orbit with positive angular velocity is shown in Fig. 5. (For convenience, the bifurcation diagram starting from its S_2 -conjugate rotational orbit with negative angular velocity is omitted.) The S_1 -symmetric rotational orbit of period 1 becomes unstable by a symmetry-breaking pitchfork bifurcation, which results in the birth of a pair of S_1 -asymmetric rotational orbits with period 1. (For the sake of convenience, only one S_1 -asymmetric orbit of period 1 is shown.) Then each rotational orbit with completely broken symmetries undergoes an infinite sequence of period-doubling bifurcations, accumulating at a finite critical point A_r^* ($= 12.252903 \dots$). The critical behaviors near the accumulation point A_r^* are also the same as those for the 1D maps, as in the case of the stationary points.

For $A > A_r^*$, four chaotic attractors with completely broken symmetries appear; they are related with respect to the two symmetries S_1 and S_2 . Through a band-merging process, each chaotic attractor eventually becomes composed of a single piece, as shown in Fig. 6(a) for $A = 12.32$. Four chaotic attractors with $\sigma_1 \simeq 0.36$ are denoted by c_1 , c_2 , s_1 , and s_2 , respectively. However, as A passes through a critical value ($\simeq 12.3424$) the four small chaotic attractors merge into a larger one via symmetry-restoring attractor-merging crisis. An example for $A = 12.38$ is given in Fig. 6(b). Note that the single large chaotic attractor with $\sigma_1 \simeq 0.64$ has both the S_1 and S_2 symmetries. Thus the two symmetries are completely restored through one symmetry-restoring attractor-merging crisis, which is in contrast to the case of the stationary points.

However, as shown in Fig. 7, the large symmetric chaotic attractor in Fig. 6(b) also disappears for $A \simeq 13.723$, at which saddle-node bifurcations occur. After disappearance of this large chaotic attractor, the system is asymptotically attracted to a stable S_2 -symmetric, but S_1 -asymmetric, orbit of period 2 born via saddle-node bifurcation. This stable S_2 -symmetric orbit with period 2 also exhibits rich dynamical behaviors similar to those of the stationary points. That is, as A is increased, a symmetry-breaking pitchfork bifurcation, period-doubling transition to chaos, merging of small asymmetric chaotic attractors into a large symmetric one via symmetry-restoring attractor-merging crisis, and so on are found. However, unlike the cases of the stationary points and the rotational orbits, the large symmetric chaotic attractor disappears for $A = 23.751799 \dots$, at

which the two unstable stationary points \hat{z}_I and \hat{z}_{II} become restabilized through subcritical period-doubling bifurcations. These “resurrections” of the stationary points will be described below in some details.

C. Resurrections of the stationary points

The linear stability of the two stationary points \hat{z}_I and \hat{z}_{II} is determined by their linearized equations,

$$\delta\ddot{x} + \Gamma \delta\dot{x} \mp 2\pi A \cos 2\pi t \delta x = 0, \quad (9)$$

where $- (+)$ sign of the third term corresponds to the case of \hat{z}_I (\hat{z}_{II}). (The linearized equation of \hat{z}_{II} can also be transformed into that of \hat{z}_I by just making a shift in time, $t \rightarrow t + \frac{1}{2}$.) Note that Eq. (9) is just a simple form of the more general damped Mathieu equation [14]. It is well known that the Mathieu equation has an infinity of alternating stable and unstable A ranges. Hence, as A is increased, the stationary points undergoes a cascade of “resurrections,” i.e., they will restabilize after they lose their stability, destabilize again, and so forth *ad infinitum*.

It is found that their restabilizations (destabilizations) occur through alternating subcritical (supercritical) period-doubling and pitchfork bifurcations. As examples, we consider the first and second resurrections of the stationary points. The first resurrection of \hat{z}_I is shown in Fig. 8. When A passes through the first restabilization value ($= 23.751799 \dots$), the rightmost large symmetric chaotic attractor in Fig. 7 disappears and the unstable stationary point \hat{z}_I restabilizes via subcritical period-doubling bifurcation, giving rise to an unstable orbit of period 2. Two bifurcation diagrams starting from the restabilized \hat{z}_I and \hat{z}_{II} are given in Fig. 9(a) and 9(b), respectively. Each stationary point loses its stability via symmetry-breaking pitchfork bifurcation, giving rise to a pair of S_2 -asymmetric orbits with period 1; only one asymmetric 1-periodic orbit is shown. This is in contrast to the case given in Sec. III A (compare Fig. 1 with Fig. 9), where the stationary points become unstable via symmetry-conserving period-doubling bifurcations. After breakdown of the S_2 symmetry, an infinite sequence of period-doubling bifurcations follows and ends at its accumulation point $A_{s,2}^*$ ($= 24.148001 \dots$). When A exceeds $A_{s,2}^*$, a second period-doubling transition to chaos occurs. The critical scaling behaviors of period doublings near the second critical point $A = A_{s,2}^*$ are also the same as those near the first critical point $A_{s,1}^*$.

Dynamical behaviors of the damped MO after the second period-doubling transition to chaos are shown in Fig. 10(a). As A passes through a critical value ($\simeq 24.1549$), small chaotic attractors with completely broken symmetries merge into a large symmetric chaotic attractor via symmetry-restoring attractor-merging crisis. However, the large chaotic attractor also disappears

for $A \simeq 29.342$, at which saddle-node bifurcations occur. After disappearance of the large chaotic attractor, the damped MO is asymptotically attracted to a stable S_1 -symmetric, but S_2 -asymmetric, orbit of period 1 born via saddle-node bifurcation. The subsequent evolution of the stable 1-periodic orbit is shown in Fig. 10(b). Note that it is similar to that of the rotational orbit described in IIIB (compare Fig. 10(b) with Fig. 7).

The rightmost large symmetric chaotic attractor in Fig. 10(b) appears via symmetry-restoring attractor-merging crisis for $A = 57.67$. However, it also disappears for $A = 67.076913 \dots$, at which each stationary point restabilizes again. Unlike the case of the first resurrection (see Fig. 8), this second resurrection of each stationary point occurs via subcritical pitchfork bifurcation, giving rise to a pair of unstable 1-periodic orbits with broken symmetries. The second resurrections of the two stationary points \hat{z}_I and \hat{z}_{II} and their subsequent bifurcation diagrams are shown in Fig. 11(a) and 11(b), respectively. Note that these third bifurcation diagrams are similar to those in Fig. 1. The critical scaling behaviors near the third period-doubling transition point $A_{s,3}^*$ ($= 67.104872 \dots$) are also the same as those near the first period-doubling transition point $A = A_{s,1}^*$.

IV. CRITICAL SCALING BEHAVIORS IN THE PERIOD-DOUBLING CASCADES

In this section, we study the critical scaling behaviors in the period-doubling cascades. The orbital scaling behavior and the power spectra of the periodic orbits born via period-doubling bifurcations as well as the parameter scaling behavior are particularly investigated.

The critical scaling behaviors for all cases studied are found to be the same as those for the 1D maps. As an example, we consider the first period-doubling transition to chaos for the case of the stationary points. As explained in Sec. III A, each stationary point becomes unstable through symmetry-conserving period-doubling bifurcation, giving rise to a stable S_2 -symmetric orbit of period 2. However, each S_2 -symmetric orbit of period 2 also becomes unstable via symmetry-breaking pitchfork bifurcation, which results in the birth of a conjugate pair of S_2 -asymmetric orbits with period 2. Then, each 2-periodic orbit with completely broken symmetries undergoes an infinite sequence of period-doubling bifurcations, ending at its accumulation point $A_{s,1}^*$. Table I gives the A values at which the period-doubling bifurcations occur; at A_k , a Floquet multiplier of an asymmetric orbit with period 2^k becomes -1 . The sequence of A_k converges geometrically to its limit value $A_{s,1}^*$ with an asymptotic ratio δ :

$$\delta_k = \frac{A_k - A_{k-1}}{A_{k+1} - A_k} \rightarrow \delta. \quad (10)$$

The sequence of δ_k is also listed in Table I. Note that its limit value δ ($\simeq 4.67$) agrees well with that ($= 4.669 \dots$)

for the 1D maps [9]. We also obtain the value of $A_{s,1}^*$ ($= 3.934787024$) by superconverging the sequence of $\{A_k\}$ [15].

As in the 1D maps, we are interested in the orbital scaling behavior near the most rarified region. Hence, we first locate the most rarified region by choosing an orbit point $z^{(k)} [= (x^{(k)}, y^{(k)})]$ which has the largest distance from its nearest orbit point $P^{2^{k-1}}(z^{(k)})$ for $A = A_k$. The two sequences $\{x^{(k)}\}$ and $\{y^{(k)}\}$, listed in Table II, converge geometrically to their limit values x^* and y^* with the 1D asymptotic ratio α ($= -2.502 \dots$), respectively:

$$\alpha_{x,k} = \frac{x^{(k)} - x^{(k-1)}}{x^{(k+1)} - x^{(k)}} \rightarrow \alpha, \quad \alpha_{y,k} = \frac{y^{(k)} - y^{(k-1)}}{y^{(k+1)} - y^{(k)}} \rightarrow \alpha. \quad (11)$$

The values of x^* ($= 0.015369$) and y^* ($= 0.348175$) are also obtained by superconverging the sequences of $x^{(k)}$ and $y^{(k)}$, respectively.

We also study the power spectra of the 2^k -periodic orbits at the period-doubling bifurcation points A_k . Consider the orbit of level k whose period is $q = 2^k$, $\{z_m^{(k)} = (x_m^{(k)}, y_m^{(k)})\}$, $m = 0, 1, \dots, q-1$. Then its Fourier component of this 2^k -periodic orbit is given by

$$z^{(k)}(\omega_j) = \frac{1}{q} \sum_{m=0}^{q-1} z_m^{(k)} e^{-i\omega_j m}, \quad (12)$$

where $\omega_j = 2\pi j/q$, and $j = 0, 1, \dots, q-1$. The power spectrum $P^{(k)}(\omega_j)$ of level k defined by

$$P^{(k)}(\omega_j) = |z^{(k)}(\omega_j)|^2, \quad (13)$$

has discrete peaks at $\omega = \omega_j$. In the power spectrum of the next $(k+1)$ level, new peaks of the $(k+1)$ th generation appear at odd harmonics of the fundamental frequency, $\omega_j = 2\pi(2j+1)/2^{(k+1)}$ ($j = 0, \dots, 2^k-1$). To classify the contributions of successive period-doubling bifurcations in the power spectrum of level k , we write

$$P^{(k)} = P_{00}\delta(\omega) + \sum_{l=1}^k \sum_{j=0}^{2^{(l-1)}-1} P_{lj}^{(k)} \delta(\omega - \omega_{lj}), \quad (14)$$

where $P_{lj}^{(k)}$ is the height of the j th peak of the l th generation appearing at $\omega = \omega_{lj}$ ($\equiv 2\pi(2j+1)/2^l$). As an example, we consider the power spectrum $P^{(8)}(\omega)$ of level 8 shown in Fig. 12. The average height of the peaks of the l th generation is given by

$$\phi^{(k)}(l) = \frac{1}{2^{(l-1)}} \sum_{j=0}^{2^{l-1}-1} P_{lj}^{(k)}. \quad (15)$$

It is of interest whether or not the sequence of the ratios of the successive average heights

$$2\beta^{(k)}(l) = \phi^{(k)}(l)/\phi^{(k)}(l+1), \quad (16)$$

converges. The ratios are listed in Table III. They seem to approach a limit value, $2\beta \simeq 21$, which also agrees well with that ($= 20.96 \dots$) for the 1D maps [16].

V. SUMMARY

Dynamical behaviors of the damped MO are investigated in details by varying the amplitude A . The damped MO, despite its apparent simplicity, exhibits rich dynamical behaviors such as breakdown of symmetries via pitchfork bifurcations, period-doubling transitions to chaos, restoration of symmetries via attractor-merging crises, and creation of new periodic attractors through saddle-node bifurcations. In addition to these familiar behaviors, a cascade of resurrections (i.e., an infinite sequence of alternating restabilizations and destabilizations) of the stationary points occurs. It is found that the stationary points restabilize (destabilize) via alternating subcritical (supercritical) period-doubling and pitchfork bifurcations. An infinite sequence of period-doubling bifurcations, leading to chaos, also follows each destabilization of the stationary points. The critical scaling behaviors in the period-doubling cascades are found to be the same as those of the 1D maps.

ACKNOWLEDGMENTS

The author would like to thank K. Lee for his assistance in the numerical computations. This work was supported by the Biomedlab Inc. and by the Korea Research Foundation under Project No. 1998-015-D00065.

-
- [1] V. Croquette and C. Poitou, *J. Phys. Lett.* **42**, 537 (1981).
 - [2] H. Meissner and G. Schmidt, *Am. J. Phys.* **54**, 800 (1986).
 - [3] K. Briggs, *Am. J. Phys.* **55**, 1083 (1987).
 - [4] J. Bialek, G. Schmidt, and B. H. Wang, *Physica D* **14**, 265 (1985).
 - [5] G. Schmidt, *Comments Plasma Phys. Controlled Fusion* **7**, 87 (1982).
 - [6] D. F. Escande and F. Doveil, *Phys. Lett. A* **83**, 307 (1981); *J. Stat. Phys.* **26**, 257 (1981).
 - [7] V. I. Arnold, *Ordinary Differential Equations* (MIT Press, Cambridge, 1973), p. 114.
 - [8] J. Guckenheimer and P. Holmes, *Nonlinear Oscillations, Dynamical Systems, and Bifurcations of Vector Fields* (Springer-Verlag, New York, 1983), Sec. 3.5.
 - [9] M. J. Feigenbaum, *J. Stat. Phys.* **19**, 25 (1978); **21**, 669 (1979).

- [10] C. Grebogi, E. Ott, F. Romeiras, and J. A. Yorke, Phys. Rev. A **36**, 5365 (1987)
- [11] S.-Y. Kim and K. Lee, Phys. Rev. E **53**, 1579 (1996).
- [12] J. Guckenheimer and P. Holmes, *Nonlinear Oscillations, Dynamical Systems, and Bifurcations of Vector Fields* (Springer-Verlag, New York, 1983), p. 24.
- [13] A. J. Lichtenberg and M. A. Lieberman, *Regular and Chaotic Dynamics* (Springer-Verlag, New York, 1983), p. 262.
- [14] P. M. Morse and H. Feshbach, *Methods of Theoretical Physics* (McGraw-Hill, New York, 1953), Sec. 5.2; J. Mathews and R. L. Walker, *Mathematical Methods of Physics* (Benjamin, New York, 1965), Sec. 7.5.
- [15] R. S. MacKay, Ph.D. thesis, Princeton University, 1982. See Eqs. 3.1.2.12 and 3.1.2.13.
- [16] M. Nauenberg and J. Rudnick, Phys. Rev. B **24**, 493 (1981).

TABLE I. Asymptotically geometric convergence of the parameter sequence $\{A_k\}$

k	A_k	δ_k
1	3.911 404 100 371	
2	3.929 795 227 873	4.690
3	3.933 716 964 019	4.664
4	3.934 557 747 089	4.667
5	3.934 737 918 915	4.669
6	3.934 776 506 700	4.668
7	3.934 784 773 689	4.673
8	3.934 786 542 923	

TABLE II. Asymptotically geometric convergence of the orbital sequences $\{x^{(k)}\}$ and $\{y^{(k)}\}$.

k	$x^{(k)}$	$\alpha_{x,k}$	$y^{(k)}$	$\alpha_{y,k}$
1	0.012 394 993		0.337 125 704	
2	0.016 703 927	-2.354	0.350 786 135	-3.410
3	0.014 873 276	-2.607	0.346 780 101	-2.133
4	0.015 575 414	-2.451	0.348 658 607	-2.714
5	0.015 288 893	-2.532	0.347 966 417	-2.395
6	0.015 402 057	-2.487	0.348 255 392	-2.561
7	0.015 356 562	-2.511	0.348 142 575	-2.472
8	0.015 374 678		0.348 188 212	

TABLE III. Sequence $2\beta^{(k)}(l) [\equiv \phi^{(k)}(l)/\phi^{(k)}(l+1)]$ of the ratios of the successive average heights of the peaks in the power spectra

k	l				
	3	4	5	6	7
6	18.2	22.5	21.0		
7	18.1	22.1	21.1	21.5	
8	18.1	22.0	20.7	21.6	21.4

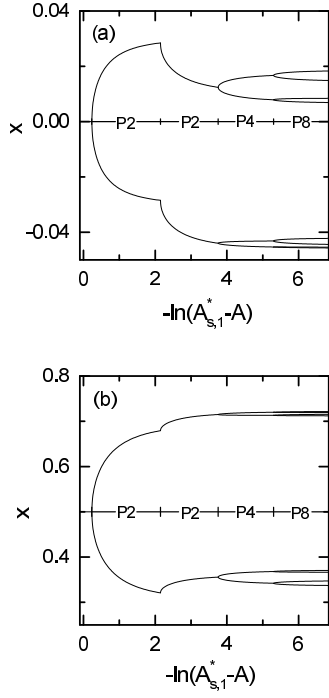


FIG. 1. Bifurcation diagrams starting from (a) the S_2 -symmetric, but S_1 -asymmetric, stationary point \hat{z}_I and (b) its S_1 -conjugate stationary point \hat{z}_{II} . The first and second P2's denote the stable A -ranges of the S_2 -symmetric and S_2 -asymmetric orbits of period 2, respectively. The other PN ($N = 4, 8$) also designates the stable A -range of the S_2 -asymmetric periodic orbit with period N .

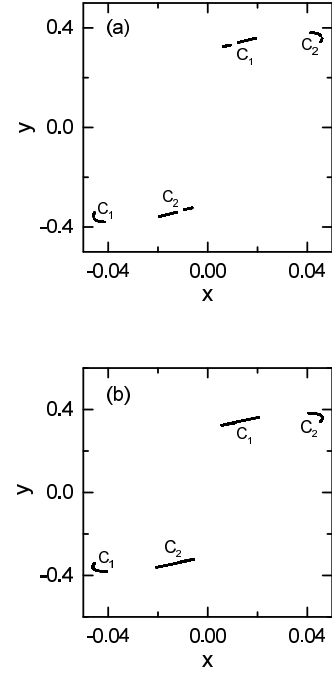


FIG. 2. Band-merging of chaotic attractors. (a) For $A = 3.937$, each of the chaotic attractors c_1 and c_2 is composed of four pieces. However, as A is increased these pieces also merge to form two larger pieces. An example for $A = 3.94$ is shown in (b).

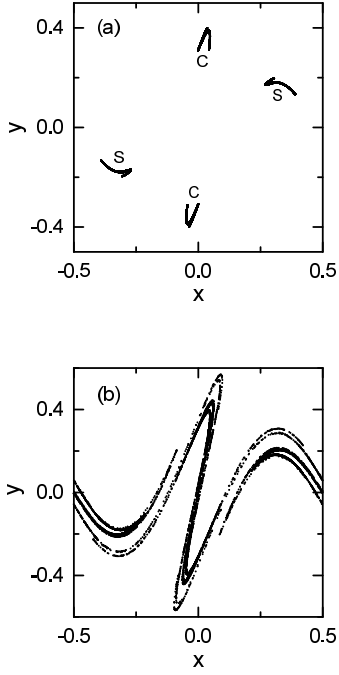


FIG. 3. Attractor-merging crises. The two chaotic attractors c_1 and c_2 in Fig. 2(b) merge into a larger one c via S_2 -symmetry-restoring crisis. For $A = 3.96$ the chaotic attractor c with the inversion symmetry S_2 and its conjugate one s with respect to the S_1 symmetry are shown in (a). These two S_1 -asymmetric small chaotic attractors c and s also merge to form a larger one via S_1 -symmetry-restoring crisis. A single large chaotic attractor with completely restored S_1 and S_2 symmetries is shown in (b) for $A = 3.98$.

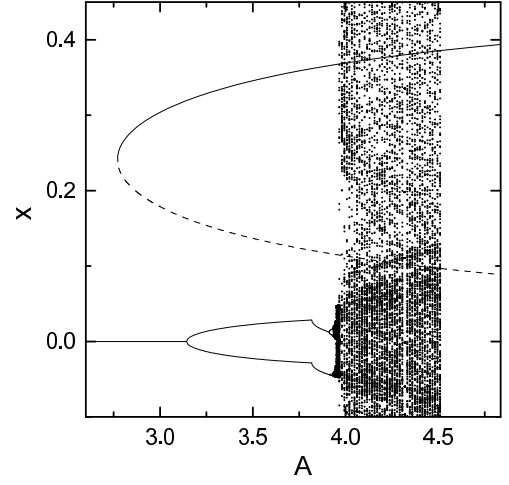


FIG. 4. Jump to a rotational orbit. The large symmetric chaotic attractor in Fig. 3(b) disappears for $A \simeq 4.513$, and then the asymptotic state of the damped MO becomes a stable rotational orbit with period 1 born via saddle-node bifurcation. Such a saddle-node bifurcation, giving rise to a pair of stable and unstable orbits of period 1, occurs for $A \simeq 2.771$ (a stable one is denoted by a solid line, while an unstable one is represented by a dashed line). A bifurcation diagram starting from \hat{z}_I is also shown.

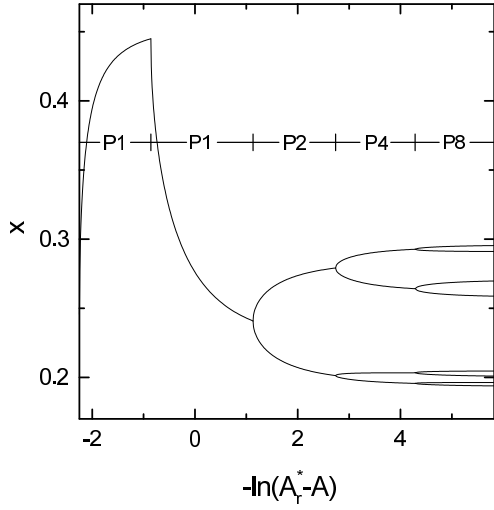


FIG. 5. Bifurcation diagram starting from the S_1 -symmetric, but S_2 -asymmetric, rotational orbit with period 1. The first and second P1's denote the stable A -ranges of the S_1 -symmetric and S_1 -asymmetric orbits of period 1, respectively. The other PN ($N = 2, 4, 8$) also designates the stable A -range of the S_1 -asymmetric periodic orbit with period N .

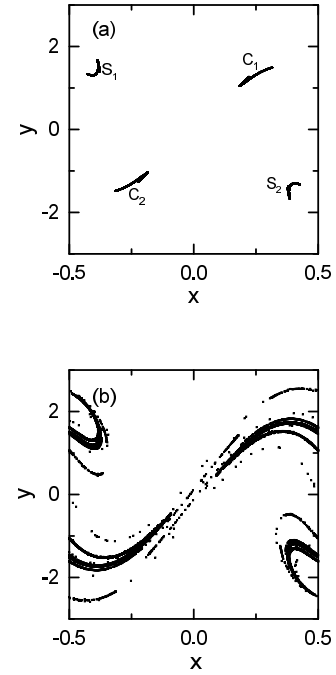


FIG. 6. Attractor-merging crisis for the rotational case. Through a band-merging process, each of the four chaotic attractors c_1 , c_2 , s_1 , and s_2 with completely broken symmetries eventually becomes composed of a single piece, as shown in (a) for $A = 12.32$. The four small asymmetric chaotic attractors merge into a larger one via symmetry-restoring crisis. A single large chaotic attractor with simultaneously restored S_1 and S_2 symmetries is shown in (b) for $A = 12.38$.

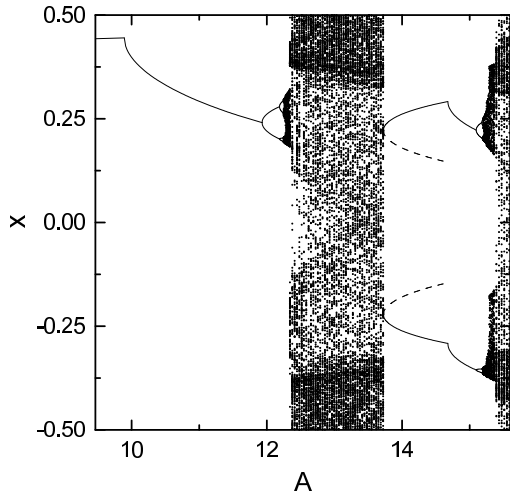


FIG. 7. Jump to an orbit with period 2. The large symmetric chaotic attractor in Fig. 6(b) disappears for $A \simeq 13.723$, at which a saddle-node bifurcation, giving rise to a pair of stable and unstable orbits with period 2, occurs. (A stable one is denoted by a solid line, while an unstable one is represented by a dashed line). Then the damped MO is asymptotically attracted to the stable S_2 -symmetric, but S_1 -asymmetric, orbit with period 2. This stable S_2 -symmetric orbit also exhibits rich dynamical behaviors similar to those of the stationary points. In the left part, a bifurcation diagram starting from a rotational orbit with period 1 is also given.

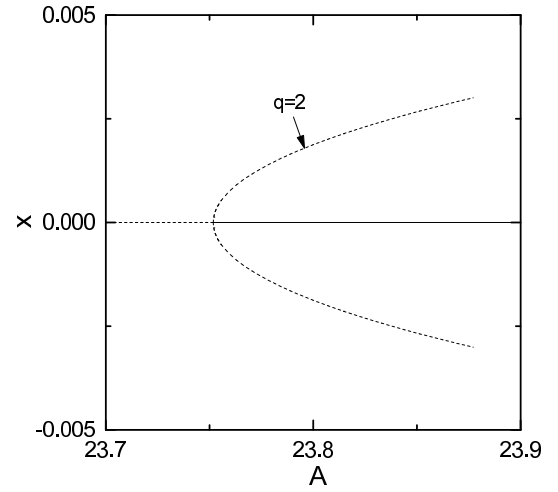


FIG. 8. First resurrection of the stationary point \hat{z}_I . When A passes through the first restabilization value ($\simeq 23.752$), the unstable stationary point \hat{z}_I restabilizes through a subcritical period-doubling bifurcation, giving rise to an unstable orbit with period $q = 2$. The solid and dashed lines also denote stable and unstable orbits, respectively.

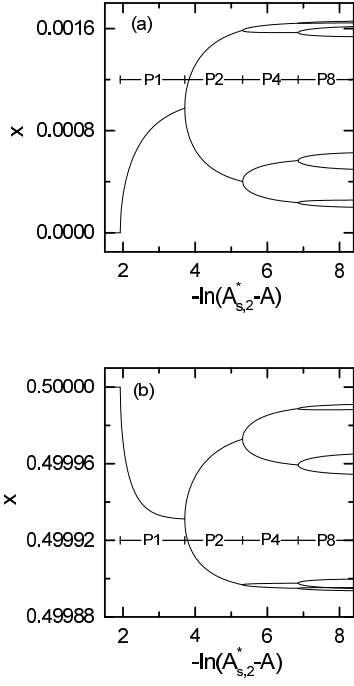


FIG. 9. Second bifurcation diagrams starting from (a) the restabilized stationary point \hat{z}_I and (b) its S_1 -conjugate stationary point \hat{z}_{II} . Here the PN designates the stable A -range of the S_2 -asymmetric periodic orbit with period N ($N=1, 2, 4, 8$).

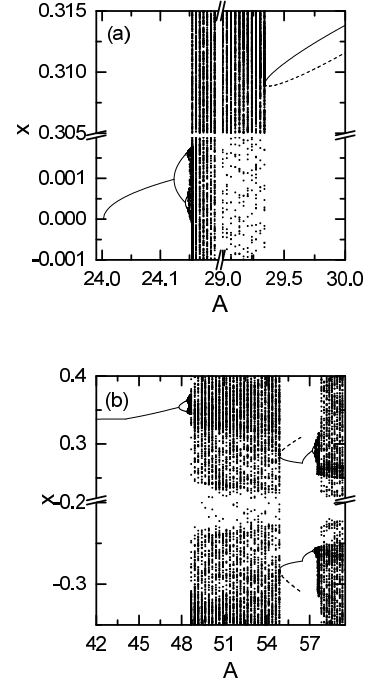


FIG. 10. Dynamical behaviors after the second period-doubling transition to chaos is shown in (a). For $A \simeq 24.1549$ small chaotic attractors with completely broken symmetries merge into a large symmetric chaotic attractor via symmetry-restoring crisis. However, this large symmetric chaotic attractor disappears for $A \simeq 29.342$, and then the damped MO is asymptotically attracted to a stable orbit of period 1 born via saddle-node bifurcation. As shown in (b), subsequent evolution of the stable S_1 -symmetric, but S_2 -asymmetric, 1-periodic orbit is similar to that of the rotational orbit shown in Fig. 7. Here the solid and dashed lines also denote stable and unstable orbits, respectively. For other details see text.

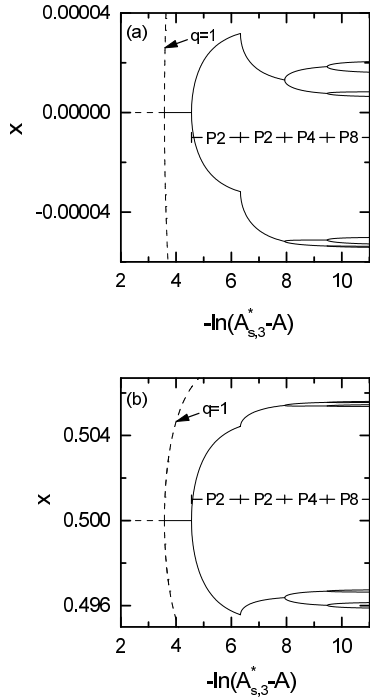


FIG. 11. Second restorations of the stationary points and third bifurcation diagrams starting from (a) the restabilized stationary point \hat{z}_I and (b) its S_1 -conjugate stationary point \hat{z}_{II} . When A passes through the second restabilization value ($\simeq 67.08$), each unstable stationary point becomes restabilized via subcritical pitchfork bifurcation, giving rise to a pair of unstable orbits with period $q = 1$. The solid and dashed lines represent stable and unstable orbits, respectively. The third bifurcation diagrams are similar to those in Fig. 1; the symbols are also the same as those of Fig. 1.

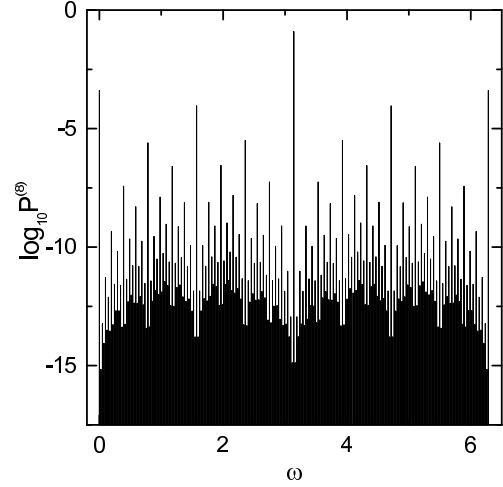


FIG. 12. Power spectrum $P^{(8)}(\omega)$ of level 8 for $A = A_s$ ($= 3.934\,786\,542\,923$).